HREM Microstructural Studies on the Effect of Steam Exposure and Cation Promoters on Vanadium Phosphorus Oxides: New Correlations with *n*-Butane Oxidation Reaction Chemistry

Pratibha L. Gai,* Kostantinos Kourtakis, D. Robert Coulson, and George C. Sonnichsen

Central Research & Development, DuPont Science & Engineering Laboratories, Experimental Station, Wilmington, Delaware 19880-0356

Received: May 20, 1997; In Final Form: September 30, 1997[⊗]

In situ environmental high-resolution electron microscopy (in situ EHREM) under different gaseous environments and ex situ HREM have been used to directly probe commercially important vanadyl pyrophosphate ($(VO)_2P_2O_7$) catalysts used in the oxidation of *n*-butane to maleic anhydride. These fundamental studies of catalyst−adsorbate interactions have shown that novel microstructural changes occur in vanadyl pyrophosphate catalysts when the catalyst is reduced, partially oxidized, or exposed to N_2 and steam environments for extended periods of 100−300 h for the first time. The microstructural changes of vanadyl pyrophosphates are related to the development of extended misfit glide shear plane defects accommodating nonstoichiometry. The complex characteristics of long-term effects of water vapor and the effect of cation promoters of iron and antimony in vanadyl pyrophosphates are explored to improve our understanding of their effects on the catalysts toward *n*-butane oxidation. Correlations of microstructural changes with reaction chemistry suggest that the changes are associated with catalyst reactivity and lattice oxygen diffusion rates.

Introduction

The selective oxidation of *n*-butane to maleic anhydride (MA) over vanadium phosphorus oxides is an important commercial process.[1−12] In the selective oxidation of the alkane to MA, the most active and selective phase is believed to be vanadyl pyrophosphate, $(VO)_2P_2O_7$ (hereafter referred to as VPO), with active centers located at the exposed (010) basal planes.[2] There are also some claims that the active phase is a combination of VPO and $VOPO_4$ phases, or a P-rich phase, or a mixture of VPO with unknown or amorphous phases.[5−7]

In addition, the effects of exposure to water vapor on the *microstructure* and performance of VPO remain a relatively unexplored area. The effect of water vapor on the catalyst equilibration is of importance since water is one of the dominant products in the selective oxidation of *n*-butane. The general consensus is that the effect of water vapor on VPO catalysts is quite complex. A detailed search of the literature (including patent literature) has shown that there are several previous chemical studies relating to the use of steam, where the reaction times used were generally short (between 30 min to approximately a few hours; some slightly longer)[18−24] with conflicting suggestions and conclusions. In some of these studies,[21] butane/air gas feed was bubbled through water and the moist feed was passed over the catalyst for short reaction times (less than a few hours), and it was suggested that the treatment could improve catalytic activity. However because of the different components in the feed (including the presence of possible impurities or solid structures), the observed improvement could not be solely attributed to the presence of water. Other studies[22,23] report *no* direct benefit by the addition of water/steam, especially to MA selectivity beyond 50% butane conversion.[23] Some patents reveal treatment of VPO with steam with a "P-compound" where the treatment was carried out sequentially for a few hours over longer periods[24] to increase the catalyst effectiveness, but effects of the addition or the nature of the P-compound were not described, whereas others describe steam treatment in the presence of cations such as Bi or other gases. In all these studies microstructural investigations of these catalysts[18−24] were not reported. Therefore despite several reports, the effect of water on VPO catalysts over longer periods is not well understood. In the present study, base (undoped) VPO catalyst was treated with water vapor at elevated temperatures for extended periods of ∼100−300 h, to understand the changes in the catalyst microstructure and their effect on the performance and long-term stability. Concurrently, cation promoter effects on the catalyst composition, microstructure, and stability in *n*-butane oxidation were also explored.

Although VPO catalysts have been characterized extensively by a variety of techniques, these studies are primarily postreaction examinations of static samples which are not the same as directly observing dynamic catalysts under operating environments at elevated temperatures. Therefore considerable uncertainty exists as to the nature of reaction mechanisms, evolution of surface disorder (defects) due to reaction, redox couples, and active sites. Recently, a novel in situ environmental cell high-resolution electron microscope (EHREM) has been developed that permits *direct* probing of live gas−catalyst interactions at elevated temperatures at the atomic level.[8] Dynamic transformation of the precursor $VOHPO_4 \cdot {}^1/_2H_2O$ to VPO has been carried out directly for the first time in the EHREM.[12] The atomic scale studies provide fundamental evidence concerning the nature of the topotactic transformation of VHPO to VPO, with no intermediate amorphous, or other, phases and reveal that atomic periodicity is maintained throughout the material. In the present study, dynamic effects of steam and other environments on the catalyst structure are examined to understand the evolution of stuctural disorder and are compared.

Experimental Procedures

A variation of an organic method[13] was used to synthesize the catalyst precursors. Vanadium pentoxide and anhydrous phosphoric acid (prepared by combining P_2O_5 with aqueous phosphoric acid) were refluxed in 11:1 isobutyl alcohol/benzyl

* To whom correspondence should be addressed.

[⊗] Abstract published in *Advance ACS Abstracts,* November 1, 1997.

S1089-5647(97)01683-0 CCC: $14.00

alcohol solvent mixtures under nitrogen. Enough phosphoric acid to satisfy a 1.1/1 P/V atomic ratio was used. Soluble pentavalent vanadyl species formed during reflux are reduced and precipitate as a blue tetravalent vanadium precursor. In the case of pure vanadium phosphorus oxides, $VO(HPO_4)\cdot^1/_2H_2O$ is precipitated. In the case of doped VPO catalysts, promoter cations were added as the soluble chlorides and alkoxides, which coprecipitate with the hemihydrate precursor.

The following calcination procedure was employed to transform the catalyst precursor to the final active phase, which in the case of pure VPO was identified as the active orthorhombic $(VO)_2P_2O_7$ phase, by powder X-ray diffraction. The unit cell data are given below. Calcinations were performed in a small, 3.5 cm fluidized bed on 60 g samples. Samples were heated to 390 °C in air for 1 h followed by heating at 460 °C for 18 h in 1.5% butane/air. Both HREM and X-ray diffraction (XRD) did not reveal any residual vanadium hydrogen phosphate hemihydrate precursor in the calcined and activated VPO catalysts.

The structure of $(VO)_2P_2O_7$ is shown in Figure 1a.[14] It is generally agreed that the structure is orthorhombic,[14] with $a = 16.594$ Å, $b = 7.76$ Å, and $c = 9.588$ Å (V(Å^3) = 1235) and 1 Å = 0.1 nm. Pairs of edge-sharing VO_6 octahedra are connected along the *b*-axis to form double chains of VO_6 octahedra sharing opposite oxygen corners. Pyrophosphate groups link the double chains into a three-dimensional network.

Studies of Effects of Exposure to Steam and Other Environments on VPO Catalysts and Correlations with *n*-Butane Oxidation Reaction Chemistry. We have probed dynamic reduction and partial oxidation reactions on the calcined and activated complex VPO catalysts using our recently developed novel environmental cell high-resolution electron microscope (EHREM) under controlled gas environments and temperatures. For EHREM, a high-resolution 300 kV Philips CM30 has been extensively modified with the introduction of a fully integrated and permanently mounted environmental cell (ECELL) system which is a chemical microreactor placed inside the EM column.[8] The method allows direct (in situ) visualization, on the atomic scale, of live catalytic reactions under gas environments and at elevated temperatures and records dynamic events in real time (with a low light level TV camera and video recorder connected to the EHREM). Very low beam currents and imaging conditions normally used for zeolites[15] were used to eliminate any beam effects, and none were detected. Blank experiments (without the beam) were also performed on catalyst samples (with the beam switched on for a few seconds only for recording) to confirm the in situ data. A conventional chemical reactor type gas manifold is used to select gas or vapor input to the ECELL, to control flow rates, and to exchange gases or to purge and evacuate the reaction chamber. Both in situ EHREM and parallel chemical reactivity tests were performed in butane, and alternatively in He, N_2, and steam as well as in partial oxidation environments of 1.5% butane/air mixture, at temperatures of ~400 °C, to directly explore nucleation and development of dynamic catalyst microstructure and its correlation with reaction chemistry. Electron diffraction, electron-stimulated energy-dispersive X-ray spectroscopy (EDX) for high-precision composition analysis and high-resolution low-voltage SEM (LVSEM) were also employed with HREM to complement the data. Exposures of the catalyst to steam for extended periods of hundreds of hours were carried out in a tube furnace to understand the relationship between the microstructure, performance, and long-term stability of steam treated VPO catalysts using the following procedures.

The steam treatment experiments were initially performed at ~360 °C on VHPO which was calcined and activated to form

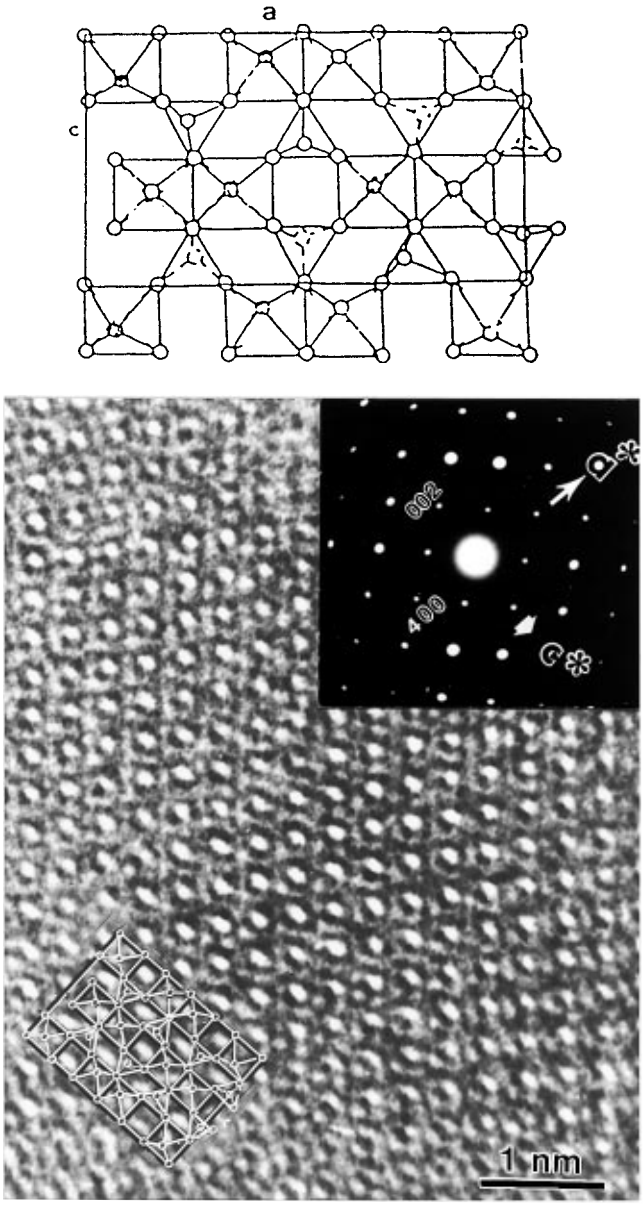

Figure 1. (a) Structural schematic of $(VO)_2P_2O_7$ (VPO). Pairs of edge-sharing VO_6 octahedra are connected along the *b*-axis, with pyrophosphate groups linking the chains of VO_6 octahedra. (b) Environmental high-resolution electron microscopy (EHREM) atomic structure of (010) VPO in butane environment, with the associated electron diffraction (ED), inset (RT), showing an ordered structure.

the $(VO)_2P_2O_7$ phase. Experiments were performed in a 3 in. fritted quartz tube placed in a vertical tube furnace. Steam was generated by using an Isco syringe pump to feed water into a vaporizer. Following each experiment, the tube was purged with nitrogen for 20 min and quenched to room temperature (5−10 min) under nitrogen flow. Surface area measurements were carried out according to the BET method, using N_2 at −195 °C.

Results

Microstructural data and reaction chemistry of the catalysts following treatments in the various environments are described and compared in the following paragraphs. The EHREM atomic structure of (010) VPO in butane at room temperature (RT) is shown here in Figure 1b, with the electron diffraction (ED). The dynamic reduction of the catalysts in butane at ~390−400 °C showed two types of extended structural defects at ~80° to each other (e.g. dark microstructural features shown at A and

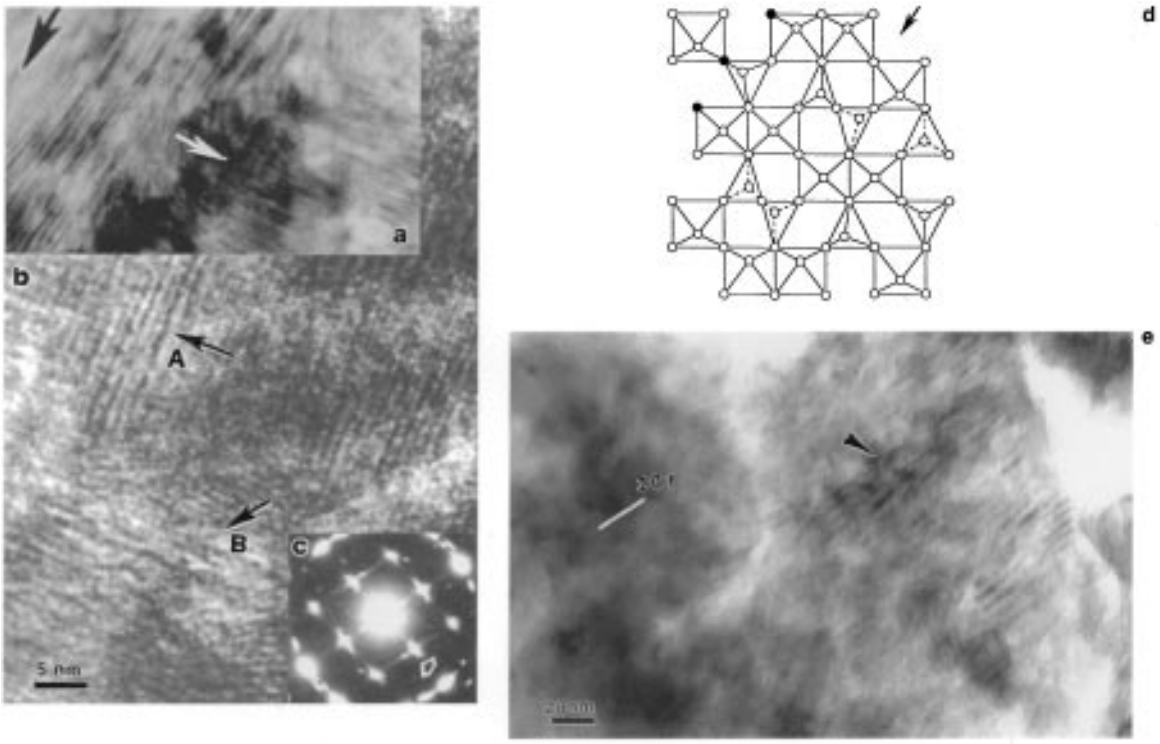

Figure 2. EHREM in situ direct probing of butane molecules−VPO catalyst interactions at ~400 °C, elucidating defect formation along ⟨201⟩ directions and growth in VPO after a few hours: (a) the two sets of symmetry-related extended defects (dark microstructural features arrowed) in diffraction contrast; (b) the same defects in high resolution; (c) the associated ED showing streaks (indicative of disorder, arrows) around the Bragg reflections, along the ⟨201⟩ directions; (d) the structural model for the extended defects deduced by detailed analyses of the in situ EHREM studies. The defects are glide shear plane defects formed by a novel glide shear mechanism and accommodate the misfit between the reduced surface layers of the catalyst containing anion vacancies and the underlying VPO;[30] vacant anion sites are indicated by filled circles; (e) in situ EHREM studies of the VPO catalyst in 1.5% butane/air environment, showing the presence of smaller concentrations of defects (imaged in a 201 reflection, arrowed), indicating a slight reduction of the catalyst surface. The figure shows disordered VPO.

B in Figure 1b), in an otherwise clean VPO matrix. They are along the two symmetry-related ⟨201⟩ directions (which are ~80° to one another). The defects were observed to nucleate near the surface and extend into the bulk as a function of reduction time. Figure 2a,b shows the defects after a few hours, in diffraction contrast and in high resolution, respectively. The associated ED shows streaks around the Bragg reflections and are along ⟨201⟩ (c). Under the reducing conditions, lattice oxygen loss due to the catalyst reduction leads to the formation of anion vacancies. Detailed analysis of the *nature* of these complex structural defects has been reported elsewhere[11] and has shown that the extended defects are (201) misfit glide shear plane defects, formed by a novel glide shear mechanism to accommodate the shape misfit between the reduced surface layers of VPO containing anion vacancies and the underlying bulk VPO. Novel misfit glide shear defect process in operating catalytic oxides was first discovered by Gai[16,17] (Gai's mechanism, which now appears to be a fundamental, effective, and pivotal process in selective oxidation catalysis by oxides generally for accommodating nonstoichiometry[11] and this misfit glide shear mechanism, based on glide defects relieving misfit strains between catalyst surface layers containing anion vacancies and the underlying unreduced bulk oxide, preserves active Lewis acid sites at the catalyst surface for catalysis). The formation of these defects was also observed by in situ EHREM in N_2 and He, which are mildly reducing environments.

The anion vacancies lie in the basal plane between corner-sharing vanadyl octahedra and phosphate tetrahedra. The defect regions thus correspond to a slightly anion-deficient defect-pyrophosphate phase, the structure of which is shown in Figure 2d, with pyrophosphate groups sharing corners similar to metaphosphate $(PO_3)_n$ groups. These local glide shear defect regions which maintain the anion vacancies (V^{3+} phases) do not change the overall VPO structure under the operating conditions, and therefore these local changes are not clearly visible in X-ray diffraction. Electron diffraction and electron microscopy (real-space crystallography) are essential to observe these reaction mechanisms directly. Following in situ studies of the catalyst in 1.5% butane/air, the defects are still observed in some areas (Figure 2e, in a (201) reflection), suggesting that a slight surface reduction of the catalyst occurs even in the presence of gas oxygen. The defects however are in significantly lower concentrations compared to the catalysts reduced with *n*-butane. This may be due to the reoxidation of many of the defects upon exposure to cofed oxygen in the gas mixture. These structural defects were also observed following exposure of the catalyst to steam in in situ experiments. The effect of steam on the catalyst is described in the following section.

TABLE 1: Steam Treatment of VPO Catalyst

sample no.	% steam	temperature, °C	time, h	surface area, m^2/g
1	31	457	24	14
2	31	355	92	25
3	42	355−362	312	23
4	0	355−362	312	n/a
5 $(VO)_2P_2O_7$				30

Table 1 summarizes the conditions for the steam treatment and surface area data. A parallel heating experiment in nitrogen for 312 h (sample 4) served as a control sample for the 312 h steam calcination to determine the effect of water vapor during the heating procedure.

In powder X-ray diffraction (XRD) data of samples treated for shorter time periods (sample 2) the effects of steam treatment were less noticeable, which may relate to the slow crystallization

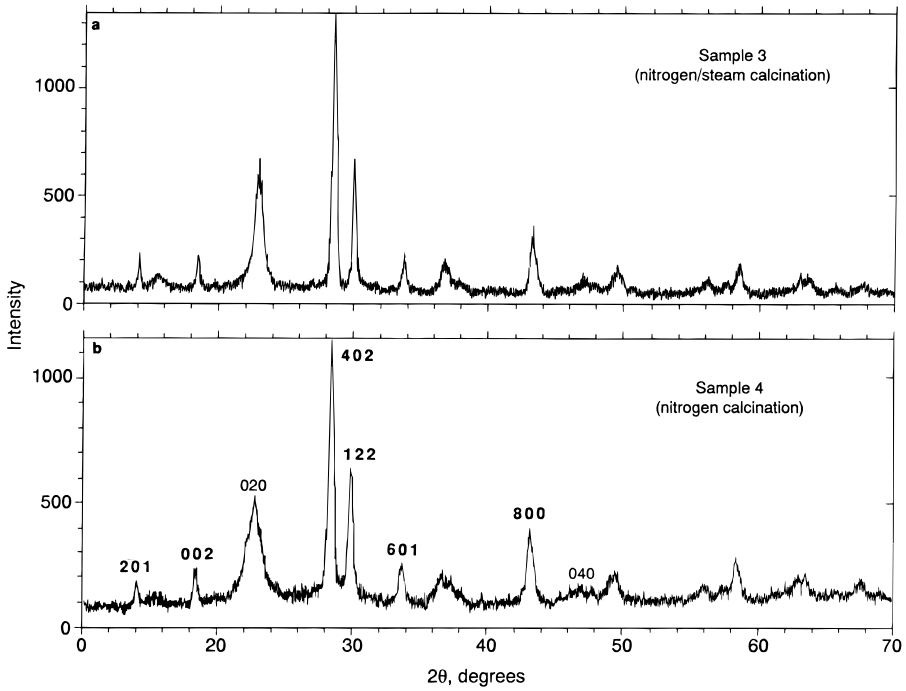

Figure 3. XRD of samples 3 and 4.

TABLE 2: Continuous Fixed Bed Microreactor Measurements

			1.5% butane/air (360 °C) % selectivity at			
sample	k, s^{-1a}	k, g/(m^2 s)	20%	40%	60% conv.	1.5% butane/N_2 maleic capacity, mmol/g catalyst
2	2.75	0.110	78	75	71	2.22
3	3.07	0.134	79	78	73	1.23
4	3.35		77	77	74	6.06
5	3.39 ± 0.22	0.113	82	80	77	4.95 ± 0.58

[a] The rate constants have been normalized to $T = 360$ °C assuming an activation energy of 25 kcal/mol.

TABLE 3: Pulsed Microreactor Data for Steam-Treated Vanadium Phosphate

		after 20 butane pulses	
sample	k, s^{-1}	conversion	MA sel.
2	2.65	16	21
3	2.05	11	9
4	3.68	21	33
5 (base VPO)	5.98	20	33

of the catalyst in the presence of water vapor at elevated temperatures. In samples reacted for extended periods in steam a modest decrease in the diffraction line widths was apparent (e.g. in sample 3), qualitatively correlating with the surface area decrease measured by N_2 BET. Figure 3a,b shows examples of XRD data for samples 3 and 4, respectively.

Rate constants were measured in a microreactor on 1 g of catalyst at temperatures between 358 and 363 °C, in 1.5% butane/air. The rate constants represent a pseudo-first-order rate constant for the disappearance of butane. Catalyst bed volumes were used in these calculations. Changes in bed porosity should be minor and should not change the relative rate constants for comparisons between catalysts. Where possible, the intrinsic rate constants are also tabulated based on N_2 BET surface area measurements. "Maleic anhydride capacities" are also tabulated, and represent the total amount of maleic anhydride liberated by reduction of each sample with a constant flow of 1.5% butane/N_2 at 360 °C. Prior to this reduction, the sample had been treated in air at 360 °C for 30 min.

A comparison of the apparent first-order rate constants tabulated above reveals that the activity of the VPO catalyst (sample 5) and the control VPO sample calcined in nitrogen for 312 h (sample 4), are nearly equal. Both steam-treated catalysts show diminished activities in 1.5% butane/air, but their intrinsic rate constants based on the BET surface area measurements are essentially equal. In the absence of cofed oxygen, marked effects are observable. The maleic anhydride capacities measured in 1.5% butane/N_2 also are diminished for the steam-treated catalysts and correlate with reactor data described in the following section.

Pulsed Microreactor Measurements. Table 3 summarizes results for the evaluation of these catalysts in a pulse microreactor at 380 °C. The pulse microreactor evaluations were carried out by injecting 0.05 mL pulses of *n*-butane using a gas sampling valve contained in an oven at 170 °C into a stream of helium flowing over 0.5 g of catalyst in a reactor heated to 380 °C. The effluent of the reactor passes through a thermal conductivity detector and then through a sample loop. When the pulse was in the sample loop, as determined by the thermal conductivity detector, it was injected into a gas chromatograph for analysis of the reaction products. The rate constants are obtained by introducing pulses of butane over the catalyst at three different flow rates, while the catalyst is reoxidized after each butane pulse with eight pulses of air at a constant flow rate. The behavior of the surface-reduced catalyst is determined by introducing successive butane pulses at 10 min intervals over the catalyst without reoxidation. Butane conversion and selectivity to maleic anhydride decrease after each pulse. *n*-Butane conversion and selectivity to maleic anhydride of the catalyst as it is reduced with successive butane pulses is shown in Figure 4a,b. The oxygen removed, or the degree of total catalyst reduction, can be calculated from *n*-butane conversion and selectivities to various oxdation products. The oxygen removed at each *n*-butane pulse is tabulated in units of micromoles oxygen reacted per gram of catalyst. Initial vanadium oxidation states were measured by redox titrimetry using a procedure similar to that of Nakamura et al.[25] The initial

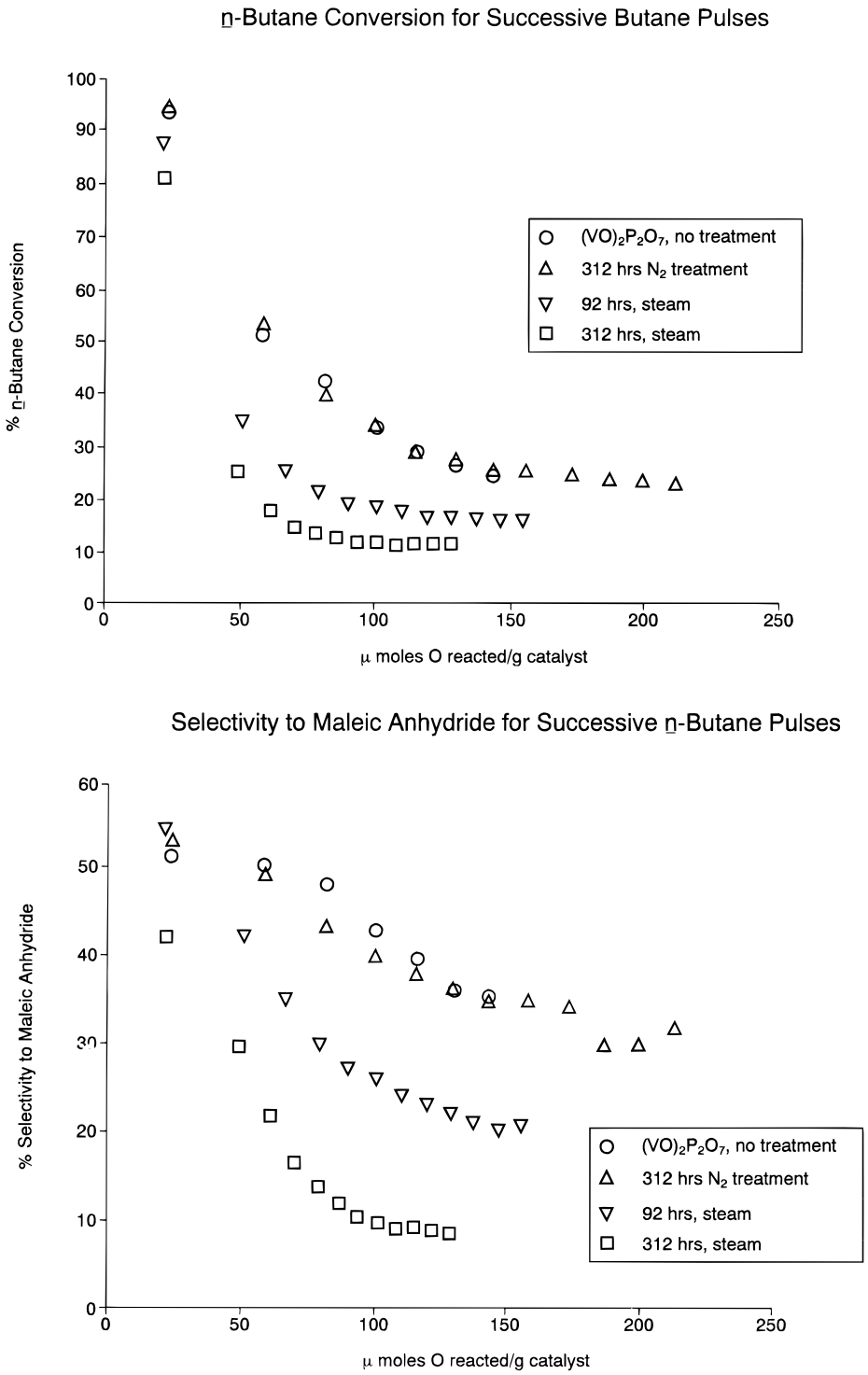

Figure 4. (a) Conversion; (b) selectivity to maleic anhydride, for successive *n*-butane pulses.

vanadium oxidation states of both steam-treated and nitrogen-calcined catalysts, as determined by this procedure, are 4.00 ± 0.01. In Figure 4a,b, a calculated value of 82 mmol oxygen (O) reacted/g catalyst is equivalent to a vanadium oxidation state change of 0.025 (3.975 ± 0.01).

Rate constant data obtained from this reactor system indicate a loss in activity for the nitrogen-calcined catalysts (sample 4) and for catalysts heated in water vapor (samples 2 and 3). Significant differences in activity between sample 4 (nitrogen-calcined VPO) and sample 5 are observed from these experiments. It is interesting that differences in catalyst activity between these samples are not observed from microreactor evaluations performed in 1.5% butane/air, described in Table 2. The lack of cofed oxygen during the pulse reactor rate constant evaluations should lead to catalyst reduction during the measurements and could account for these activity differences.

Marked differences in catalytic behavior upon reduction are more dramatically indicated from the pulse reactor during catalyst reduction with consecutive pulses of *n*-butane. At the 20th pulse of *n*-butane, sample 3, which was treated in an atmosphere of 42% steam for 312 h, is significantly less active and selective than VPO (sample 5) or VPO calcined in nitrogen (sample 4). These results qualititatively agree with continuous fixed bed evaluations (described in the previous section) in 1.5% butane/nitrogen.

This is further demonstrated in Figures 4a,b, in which the micromoles oxygen reacted per gram of catalyst is plotted against *n*-butane conversion and selectivity to maleic anhydride. (Plots of surface area against *n*-butane conversion and selectivity to MA were identical.) It is clear that important differences in both conversion and selectivity are observed. Samples 2 (92 h, steam) and 3 (312 h, steam) are clearly different from the base "VPO" catalyst, sample 5 ($(VO)_2P_2O_7$) and the control VPO catalyst calcined for 312 h in nitrogen. Both steam-treated samples (samples 2 and 3) are less active and selective to maleic anhydride than samples 3 and 4 as they are reduced, indicating that the active sites of these have been depleted of oxygen. The plateau observed from these reduction graphs reflects a depletion of reactive surface oxygen, so that the reaction is limited by lattice oxygen diffusion. The lower plateaus observed for both steam-treated catalysts suggest lower oxygen anion diffusion rates for the steam-treated catalysts compared with the VPO control samples. The relative positions of the plateaus reached with these curves should not be dependent on small changes in the initial oxidation states of the catalyst samples.

Microstructures of Steam-Calcined VPO and Correlation with Reaction Chemistry. Electron microscopy investigations have revealed that steam plays an important role in the development of the disordered VPO structure. The key observation from in situ electron microscopy experiments in steam at ~390 °C is the evolution of extended glide shear defects of the type we have observed in vanadyl pyrophosphate (VPO) reduced in butane in {201} orientations. The defect concentration was found to be higher in steam than in samples reacted in butane and N_2 under similar conditions. This novel result is discussed in the following sections.

Comparisons of the control sample and steam-treated samples from the reactor studies indicate that the steam/VPO samples contain a higher concentration of the defects, confirming in situ observations that steam accelerates their formation. The defect concentration in steam also increases considerably as a function of time: for example, steam/VPO samples reacted for 312 h have a higher defect density than the sample reacted for 92 h. In the steam/VPO samples steamed for 24 and 92 h, streaking (disorder) from the defect regions is found to be predominant, suggesting that long-range order has not yet been achieved. By measuring the number of defects per formula unit (in Figure 2b), the *local* oxidation state of V in these defective regions may be estimated to be ~3.7−3.8 (i.e. close to 4^+), dispersed in a VPO matrix with V^{4+}, if the V^{3+} states are not terminated by hydroxyl groups. The percentage of misfit glide shear defects observed, the anion deficiency, and the averaged oxidation state (of the defects and bulk) changes fall in the range of 0.02 valence units. Vanadium oxidation state measurements, by redox titrimetry which give an overall oxidation state, are not capable of distinguishing changes in vanadium oxidation states smaller than these valence units. However, it is also possible that although the misfit glide shear defects form by a redox mechanism, anion vacancies and V^{3+} states are oxidized to V^{4+} and terminate with hydroxyl species.

In the steam/VPO samples reacted for 312 h, platy formation of crystallites is indeed visible in some areas of the samples along the ⟨201⟩ defect directions: this suggests that in a prolonged exposure long-range order (leading to a new, slightly anion-deficient phase) is essentially reached in those crystals. The misfit glide shear is a mechanism for these larger microstructural changes which occur with time in the catalyst and may be important in the long-term stability. Since such plates are also formed in prolonged reduction in butane,[11] they appear to be anion-deficient structures ($VPO_{4.33}$). LVSEM showed that

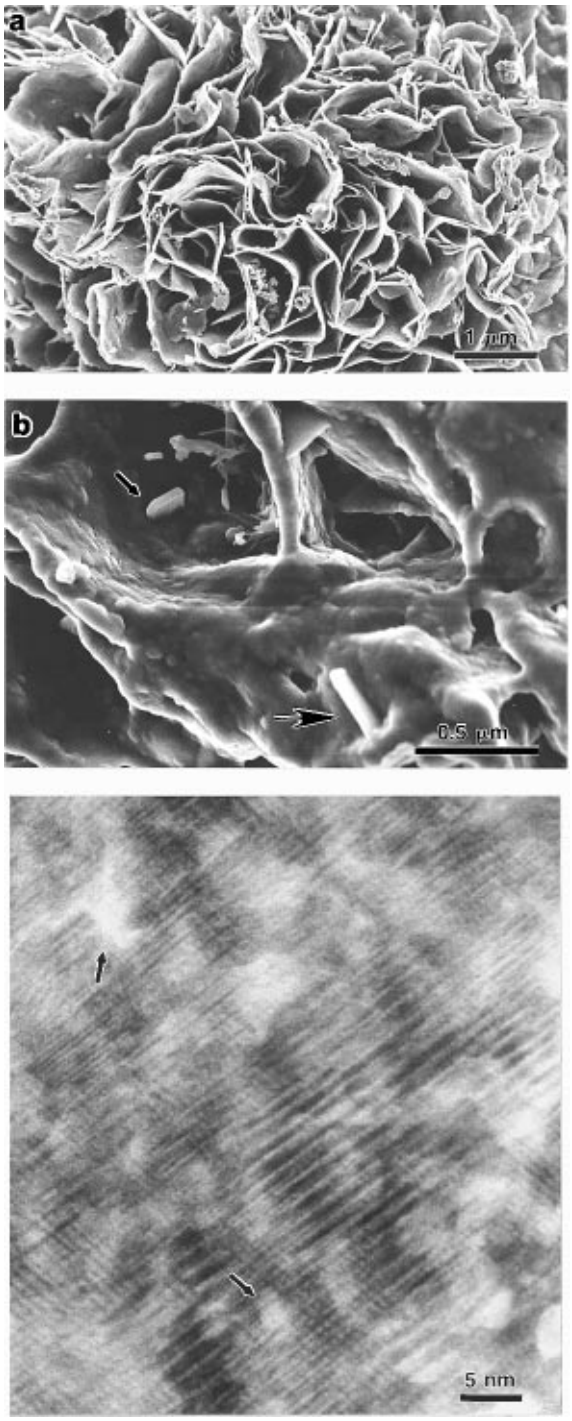

Figure 5. Steam interactions with VPO catalyst: (a) low-voltage SEM (LVSEM) of base VPO; (b) LVSEM of the steamed-VPO catalyst with microcrystals (plates, arrows); and (c) HREM of VPO crystals covered with the extended glide shear defects and porosity (arrows).

in some areas rosettes were decomposed into microcrystals, resulting in porosity. Figure 5 summarizes microstructural observations in steam: part a shows LVSEM of base VPO; part b shows LVSEM images of steamed catalyst with microcrystals/plates (arrows); part c shows a HREM image of crystals covered with glide shear defects and porosity (arrows) in steam. The inset shows a large concentration of glide defects at lower magnification. Furthermore, the study of the VPO sample heated in N_2 has shown the presence of glide shear defects, but in lower concentrations compared to those treated in steam under similar conditions of temperature and time. Electron diffraction showed diffuse streaking due to the defects (similar to that shown in butane in Figure 2c), suggesting disorder.

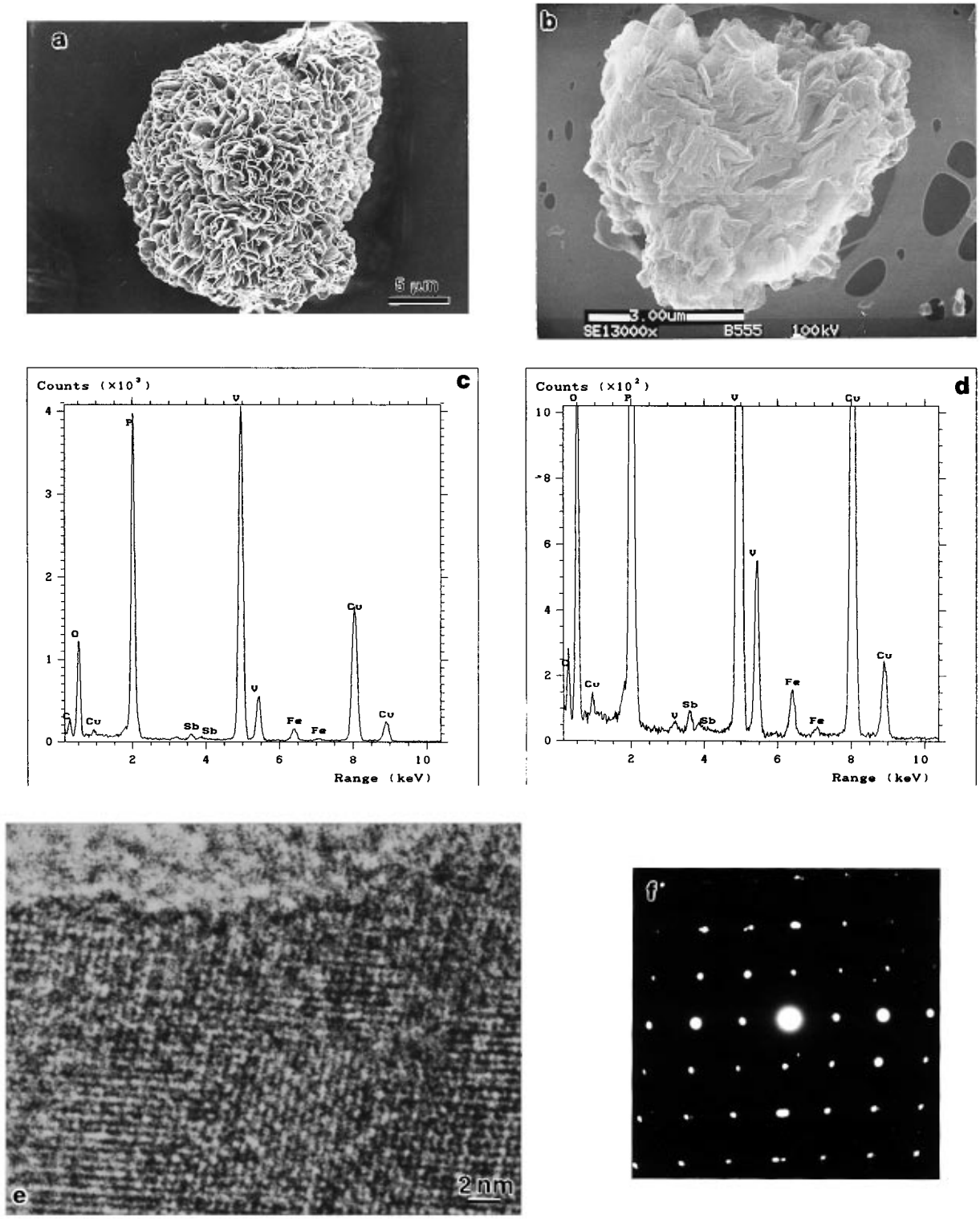

Figure 6. High-resolution and analytical electron microscopy of promoted $(V_{0.9}Fe_{0.05}Sb_{0.05}O)_2P_2O_7$ catalyst ((Fe,Sb)VPO): (a) surface morphology of base VPO; (b) morphology of the (Fe,Sb) VPO with smoother structure; (c) electron-stimulated high-precision X-ray spectroscopy in the electron microscope (EDX) for microchemical analysis of the promoted catalyst showing the presence of Fe and Sb in solid solution; (d) the spectral area at higher magnification; **(e)** HREM showing a well-ordered single phase formation of (Fe,Sb)VPO; there is no evidence of amorphous or secondary phases on the surface of the catalyst crystals; (f) the corresponding electron diffraction.

Discussion

Our direct in situ electron microscopy observations of steam, butane, and butane/air interactions with the catalyst and analyses of the steam-calcined and control experiments indicate that in all these environments the VPO crystal surface is slightly altered and the crystal is continuously changing to the (201) lower energy stable configuration. The studies show that during the operation of the catalyst some anion vacancies are formed which lie in the basal plane. The slight reduction of the catalyst surface leads to restructuring via the formation of (201) glide shear defects which accommodate the misfit strains between the reduced layers containing anion point defects and the underlying bulk VPO. These defect sites may be important in oxidation and anion diffusion. Under partial oxidation conditions, the novel glide shear process provides an effective mechanism to accommodate small deviations in stoichiometry, without the

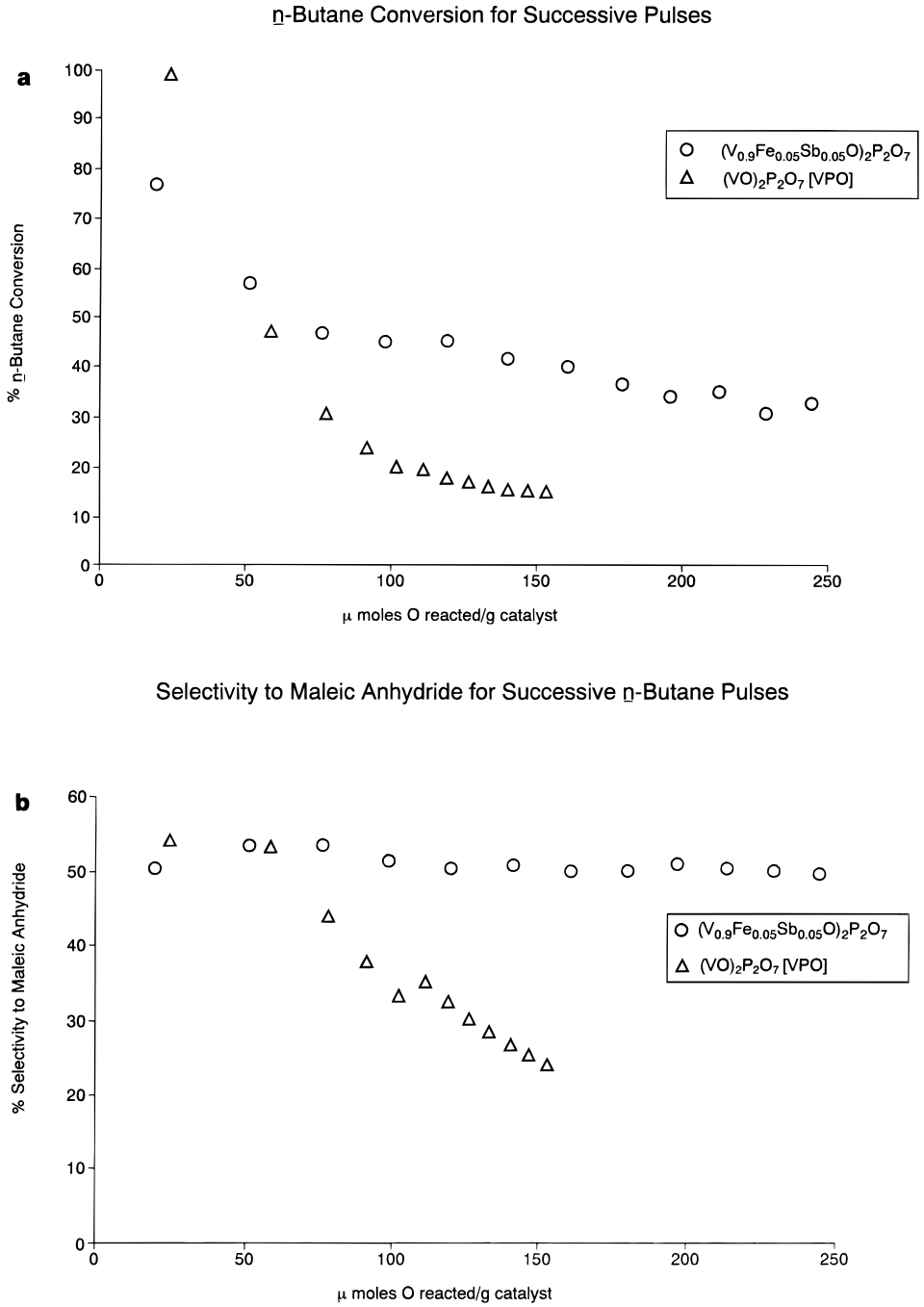

Figure 7. (a) Pulse reactor data for promoted catalyst: *n*-butane conversion for successive butane pulses compared with those of base VPO. (b) Selectivity to maleic anhydride for successive butane pulses.

collapse of the VPO lattice. Only the local symmetry is altered at the defect boundary between the surface and bulk VPO due to the crystal glide. The microstructural and reactivity data suggest that steam especially enhances the extent of reduction and catalyst reconstruction (i.e. the formation and growth of the glide shear defects leading to crystallite growth). The reasons for these are unclear to us at present, but we propose the following speculations for the observed microstructure and catalyst performance upon long exposures of VPO catalysts to steam.

As described in the preceding sections, we have observed increased structural defects upon exposure to steam as shown in Figure 5. Over extended periods the microstructural changes leading to crystallite growth would reduce the active VPO surface content and manifest in the observed decrease in the catalyst performance affecting the useful life of the catalyst. It is possible that in the presence of water some of the catalyst surface sites are occupied by hydroxyl groups. This hydroxylated surface might inhibit further chemisorption of oxygen and reduce sites capable of oxidizing the alkane, resulting in a decrease in the rate of butane oxidation. These possibilities are discussed below.

Microreactor data show that prolonged steam treatment of VPO results in a significant loss in acitivity and selectivity as the catalyst is reduced in *n*-butane; the activity decline is not apparent during evaluations in 1.5% butane/air. This implies that steam treatment has reduced the population of sites capable of oxidizing butane to maleic anhydride in the absence of gas-phase oxygen during catalyst reduction. This is accompanied by a loss of N_2 BET surface area and a decrease in XRD line width, which together are consistent with electron microscopy data indicating crystallite growth and an increase in the extended

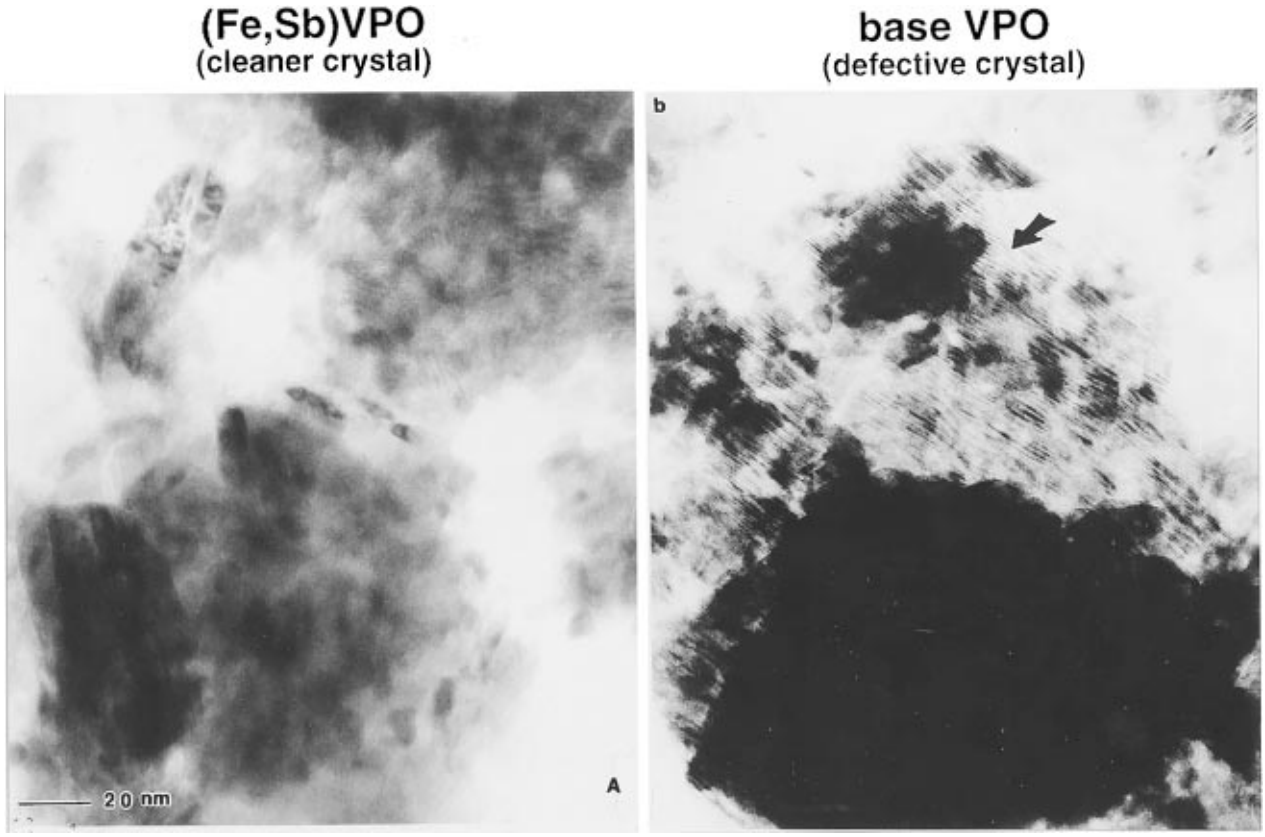

Figure 8. Butane reaction for a few hours: (a) (Fe,Sb)VPO; (b) base VPO.

glide shear defects. In the absence of cofed oxygen, it is possible that the chemisorbed water prevents chemisorption of any trace oxygen in the butane/N_2 stream, inhibiting the partial reoxidation of the catalyst. It may also be due to the fact that the redox and recontruction of the catalyst depend upon hydroxylation state of the catalyst surface. The loss in activity and selectivity of the catalysts during prolonged reduction indicates a loss in catalyst lattice oxygen carrying capacity in the absence of cofed oxygen, which is a consequence of decreased lattice oxygen diffusion rates. The oxygen diffusion rates are most diminished for steam-treated catalysts and roughly correlate with the formation and increased number of glide shear defects extending throughout the sample in prolonged treatments. In prolonged reduction with *n*-butane in the absence of cofed oxygen, the large number of misfit extended glide shear defects, extending throughout the sample, tend to order into new plate crystals which correspond to a new, slightly anion-deficient phase, and may interfere with oxygen anion transport to catalyst surfaces.

Although glide shear defects are present in all the environments to a varying degree, the extent of ordering (condensation into a new phase) of a large number of glide defects especially in the absence of cofed oxygen may be important in understanding the loss of activity and selectivity in steam compared to the samples reacted in *n*-butane and nitrogen. Steamed samples have more plates due to ordering of a larger number of the defects. Comparison of the activity data of steam-treated samples with those of the N_2-treated and unmodified VPO samples suggests that a small number of the disordered glide shear defects is sufficient to accommodate slight stoichiometric deviations in selective oxidation reactions and for facilitating operation of the catalyst. Inhibiting irreversible reduction of the sites capable of maleic activity by controlling the concentration and ordering of the defects is largely accomplished in the presence cofed oxygen in 1.5% butane/air.

Effects of Cation Promoters on the VPO Catalyst System in *n*-Butane Oxidation Chemistry: $(V_{0.9}Fe_{0.05}Sb_{0.05}O)_2P_2O_7$. The role of cation promoters on the microstructure and stability of VPO catalysts in *n*-butane catalysis is of major importance. Although several studies have been cited in the literature[26,27] on the specific activity and MA selectivity of promoted VPO catalysts, *no direct* evidence for the formation of solid solutions with VPO has been reported. Understanding of the location and of the complex role of promoters is therefore lacking. We have synthesized a novel (Fe,Sb) promoted catalyst system[28] and have probed the structure and chemistry of the catalyst by atomic scale HREM imaging in conjunction with composition analyses. The extent of solid solution and the promoter effect on the catalyst microstructure and stability in *n*-butane oxidation are examined in the following sections. Chemical composition spectra calibrated with standards have been obtained in the electron microscope using electron-stimulated energy-dispersive X-ray (EDX) spectroscopy from a large number of crystals.

Our studies elucidate that iron and antimony are present in solid solution in vanadyl pyrophosphate, indicating the formation of a new promoted phase isostructural with the undoped VPO. These results are summarized in Figure 6: part a shows surface morphology of base VPO; surface morphology of (Fe,Sb) VPO shown in Figure 6b appears to be smoother than VPO (Figure 6a); part c shows a high spatial resolution (2 nm) EDX microanalysis spectrum from the catalyst, indicating that Fe and Sb are present throughout in the catalyst forming a novel composition, isostructural with $(VO)_2P_2O_7$ (peaks from the Cu sample holder are also visible); part d shows the magnified spectral region showing Fe and Sb peaks more clearly; and part e shows a HREM image indicating a well-ordered promoted catalyst with the associated electron diffraction pattern (f). There is no evidence for amorphous or additional phases on the surface of the catalyst crystallites. The new composition can therefore be described as $(V_{0.9}Fe_{0.05}Sb_{0.05}O)_2P_2O_7$.

Pulse reactor data of the catalyst system are shown in Figure 7a,b. It is clear that compared to pure $(VO)_2P_2O_7$, both conversion and selectivity are improved for $(V_{0.95}Fe_{0.05}Sb_{0.05}O)_2P_2O_7$ as oxygen is removed from the catalyst. In both cases, the catalyst is exposed to consecutive *n*-butane pulses and is not reoxidized between pulses. As observed for the steam-treated catalysts, once surface oxygen is removed by reduction with *n*-butane, the reaction becomes limited by lattice oxygen diffusion and is indicated by plateaus in both conversion and selectivity for both catalyst systems during further reduction. However, the higher conversion and selectivities noted in the diffusion-limited regime which are observed to the right of Figure 7a,b clearly show that the rate of anion diffusion to the surface of $(V_{0.9}Fe_{0.05}Sb_{0.05}O)_2P_2O_7$ is enhanced compared to VPO. One explanation for the enhanced oxygen diffusion rates may be that cooperative behavior between the FeII/FeIII and Sb(III)/Sb(V) (where the promoter cations may be pinning anion vacancies), anion defects, and vanadium redox couples is important in the diffusion.

Additionally, our initial HREM studies on the promoted catalysts cycled between *n*-butane and air for a few hours have indicated that the microstructural changes due to the development of a large number of extended glide defects are less marked in these catalysts relative to pure $(VO)_2P_2O_7$ (Figure 8a,b). This suggests that the promoter cations may be pinning the anion vacancies (or oxidize them) and inhibiting the growth and ordering of a large number of the defects into *new platy* structures and thus may act to maintain the optimal anion defect concentration and surface oxidation state of the vanadium. With the present HREM methods it is not possible to image isolated anion point defects. Since the development and ordering of the defects appear to be symptomatic of further larger microstructural changes as a function of time, the presence of these promoters may help to stabilize the pyrophosphate structure.

Conclusions

The in situ EHREM studies coupled with reaction chemistry have provided insights into the nature of dynamic reaction mechanisms of VPO catalysts in *n*-butane, butane/air, and steam environments. The slight reduction of the catalyst in *n*-butane oxidation leads to restructuring via the formation of (201) glide shear defects, which accommodate the resulting nonstoichiometry. Effects of long-term exposure to steam on VPO catalysts show a marked increase in the number of glide defects which order into new anion-deficient plate crystals. Cation-promoted vanadyl pyrophosphate with a nominal composition $(V_{0.9}Fe_{0.05}Sb_{0.05}O)_2P_2O_7$ has been synthesized and compared with undoped VPO in the *n*-butane oxidation. Pulse reactor studies have indicated higher lattice oxygen carrying capacities in the promoted catalyst. Microstructural studies indicate that the iron and antimony might maintain optimal anion point defect concentration.

The in situ EHREM confirms our earlier results on simple and mixed-metal oxide catalysts that crystallographic shear planes formed during catalytic reactions which eliminate vacant sites, resulting in lattice collapse, are secondary to catalysis[16,17,29,31] and glide shear is the most effective defect mechanism in accommodating nonstoichiometry and facilitating continued operation of oxide catalysts in selective oxidation reactions.

Acknowledgment. P.L.G. thanks C. R. A. Catlow and A. K. Cheetham for the kind invitation to prepare this article. She continues to enjoy a very fruitful collaboration with Sir John Meurig Thomas on structural chemistry and catalysis of novel zeolites. She and her colleagues thank H. S. Horowitz and E. D. Boyes for technical discussions and L. G. Hanna, D. L. Smith, J. J. Borowski, D. Cline, Jr., M. Harrison, T. Fleckenstein, F. G. Gooding, and E. Jones for technical assistance.

References and Notes

(1) Hodnett, B. K. *Catal. Rev.-Sci. Eng*. **1985**, *27*, 323.
(2) Bordes, E. *Catal. Today* **1987**, *1*, 499.
(3) Centi, G. (ed. sp. vol.) *Catal. Today* **1993**, *16*, 1.
(4) Horowitz, H. S.; et al. *Appl. Catal.* **1988**, *38*, 193.
(5) Adelouahabab, F.; Volta, J. C.; et al. *J. Catal.* **1991**, *128*, 248.
(6) Koyano, G.; Okuhara, T.; Misono, M. *Catal. Lett*. **1995**, *32*, 205.
(7) Kiely, C.; Sajip, S.; Ellison, I.; Santanes, M.; Hutchings, G. J.; Volta, J. C. *Catal. Lett*. **1995**, *33*, 357.
(8) Boyes, E. D.; Gai, P. L. *Ultramicroscopy* **1997**, *67*, 219. In Situ Microscopy in Materials Research; Gai, P. L., Eds.; Kluwer Academic Publishers: Dordrecht, 1997.
(9) Gai, P. L.; Kourtakis, K. *Science* **1995**, *267*, 661.
(10) Gai, P. L.; Kourtakis, K.; Coulson, R.; Sonnichsen, G. In *Catalyst Materials for High-Temperature Processes*; Ramesh, K. S., Misono, M., Gai, P. L., Eds.; American Ceramic Soc.: Westerville, OH, 1997; Vol. 73.
(11) Gai, P. L. *Acta Crystallogr*. **1997**, *B53*, 346.
(12) Gai, P. L.; Torardi, C. C. In *In Situ Electron & Tunneling Microscopies*; Sharma, R., Gai, P. L., Gajdarziska, M., Sinclair, R., Whitman, L., Eds.; Materials Research Society: Warrendale, PA, 1996; Vol. 404.
(13) Katsumoto, K.; Marquis M. Chevon Co. U.S. Parent 4,132,670.
(14) Gordunova, Yu. E.; Linde, S. *Sov. Phys.-Dokl. (Engl. Trans.)* **1979**, *24*, 138.
(15) Gai, P. L.; Thomas, J. M.; Wright, P.; Jones, R.; Natarajan, S.; Chen, J.; Xu, R. *J. Phys. Chem*. **1992**, *96*, 8206.
(16) Gai, P. L. *Philos. Mag. A* **1981**, *43*, 841.
(17) Gai, P. L. *Catal. Rev.−Sci. Eng*. **1992**, *34*, 1.
(18) Tomita, S.; Kawakami, T.; Suwa, H.; Ihara, T., Mitsubishi Chem. Ind. Japan Patent JP 05043567 A2 930223, 1992.
(19) Ebner, J.; Andrews,W., Monsanto Co. U.S. US 5137860 A 920811.
(20) Ootake, M.; T. Kawakami, T.; Otake, M., Mitusbishi Kasei Corp. Japan Patent JP 01201016 A2 890814, 1988.
(21) Arnold, E. W.; Sundaresan, S. *Appl. Catal*. **1988**, *41*, 225.
(22) Cornaglia, A.; et al. *Appl. Catal*. **1991**, *74*, 15.
(23) Lerou J. J.; Mills, P. L. *Proceedings Process Techn. International Conference*; Weijenen, M., et al., Eds.; Kluwer Academic Publ.: Dordrecht, 1993; p 175.
(24) Click, G.; Barone, B., Denka Chem. Corp. U.S. 4515899 A 850507, 1985.
(25) Nakamura, M.; Kawai, K.; Fujiwara, Y. *J. Catal*. **1974**, *34*, 345.
(26) Bej, S. K.; Rao, M. S. *Appl. Catal*. **1992**, *A83*, 149.
(27) Hutchings, G. J.; Higgins, R. *J. Catal*. **1996**, *162*, 153.
(28) Kourtakis K.; Sonnichsen, G., U.S. Patent 543532. Kourtakis, K.; Sonnichsen, G.; Coulson, D. R.; Gai, P. L. Manuscript in preparation.
(29) Gai, P. L.; et al. *Nature* **1990**, *348*, 430.
(30) Notes: The studies[11] have shown that the displacement vector is approximately parallel to the trace of (201) planes (lies in the plane of shear) and to the defect directions.
(31) Gai, P. L. *J. Solid State Chem.* **1993**, *104*, 119.